

A constrained optimization approach to nonlinear system identification through simulation error minimization

Vito Cerone, Sophie M. Fossion, Simone Pirrera, Diego Regruto*

Abstract

This paper introduces a novel approach to system identification for nonlinear input-output models that minimizes the simulation error and frames the problem as a constrained optimization task. The proposed method addresses vanishing gradient issues, enabling faster convergence than traditional gradient-based techniques. We present an algorithm based on feedback linearization control of Lagrange multipliers and conduct a theoretical analysis of its performance. We prove that the algorithm converges to a local minimum, and it enhances computational efficiency by exploiting the problem's structure. Numerical experiments demonstrate that our approach outperforms gradient-based methods in both computational effort and estimation accuracy.

1 Introduction

System identification (SI) is the science of learning models of dynamical systems from experimental data. From a mathematical perspective, this process involves selecting a model class and estimating its parameters by solving an optimization problem. For further reading, see the works by [Ljung, 1999], [Bohlin, 2006], and [Milanese et al., 1996].

Most approaches to SI rely on prediction-error minimization, which involves identifying the model parameters by minimizing the difference between the measured output and the one-step-ahead prediction generated by the model. Prediction-error minimization methods are consistent, meaning that the parameter estimates converge to the true value as the amount of data increases, under the crucial assumption that the selected model classes for both the system and the noise are accurate; see [Ljung, 1999]. However, if these assumptions do not hold, prediction-error minimization methods may yield models with limited accuracy in system simulation; see [Zhang, 2004] and [Piroddi, 2008] for a detailed discussion of this topic.

A viable alternative formulates the parameter estimation problem as minimizing the simulation error, defined as the difference between the measured output and the output predicted by the model across the entire data set. This approach, known as *simulation-error minimization* (SEM), yields consistent estimates regardless of the measurement

noise model; see [Söderström and Stoica, 1982] and [Farina and Piroddi, 2010].

The primary disadvantage of SEM lies in the difficulty of solving the optimization problem, which is generically nonconvex. Notably, even when the system is linear time-invariant, the resulting SEM has a polynomial structure, thus remaining nonconvex; see, for example, [Cerone et al., 2012] and [Cerone et al., 2023].

In the general case of nonlinear systems, SEM is a differentiable, nonconvex minimization problem, and its standard solution relies on gradient-based optimization. Notable examples include gradient descent, pseudo-second-order algorithms, and methods based on extended Kalman filters; for a comprehensive overview, refer to [Ruder, 2016]. All gradient-based methods require computing the gradients of the output samples with respect to the model parameters. These gradients are recursively dependent, resulting in a dynamic relationship. [Narendra and Parthasarathy, 1991] explicitly leverage this relation to define an estimation algorithm. Alternatively, we can compute the gradients in closed form or through automatic differentiation; see [Baydin et al., 2018] for a recent survey. Among gradient-based methods based on automatic differentiation, we mention the backpropagation through time (BPTT) algorithm, as introduced by [Williams and Zipser, 1990], which has gained renewed popularity for identifying nonlinear systems modeled using recurrent neural networks. For further reading, refer to [Medsker and Jain, 1999] as well as [Salem, 2022].

A drawback of gradient-based methods is that the dynamic relationships among gradient samples can result in vanishing and exploding gradient issues. In essence, these problems arise from the stability of the dynamical system that governs the interactions among gradients. If the system is stable, the contribution of past samples vanishes; if it is unstable, the gradients diverge. The practical implications include convergence to inaccurate estimates and either slow convergence or instability of the identification algorithm. For further details, refer to [Bengio et al., 1994] and [Pascanu et al., 2013].

When dealing with gray-box SI, gradient-based SEM often results in highly inaccurate estimates; see, e.g., [Parrilo and Ljung, 2003] and [Prot and Mercère, 2020]. In black-box SI, the standard approach to mitigating the vanishing gradient problem involves constructing ad hoc models like long-short-term memory (LSTM) or gated recurrent unit (GRU) networks. However, LSTM and GRU tend to overfit, and their training is computationally intensive and time-consuming.

Alternatives to gradient-based optimization are

*The authors are with the Dipartimento di Automatica e Informatica, Politecnico di Torino, corso Duca degli Abruzzi 24, 10129 Torino, Italy; e-mail: {vito.cerone; sophie.fossion; simone.pirrera; diego.regruto}@polito.it

scarce. While meta-heuristic approaches, such as those proposed by [Blanco et al., 2001] and [Bas et al., 2022], are available, they are often disregarded due to high computational demands and the absence of theoretical guarantees. Furthermore, studies by [Piroddi and Spinelli, 2003] and [Farina and Piroddi, 2011] explore prediction-error minimization and a posteriori simulation-error evaluation. However, these methods exclusively apply to linearly parameterized models. [Adeoye and Bemporad, 2024] introduce a method based on constrained optimization and sequential quadratic programming (SQP). However, since SQP is a second-order algorithm that requires computing large Hessian matrices, approximate formulations are adopted.

This paper proposes a novel algorithm to address SEM identification of nonlinear input-output (NIO) models. We formulate the identification problem as a *constrained optimization* task. The cost function accounts for the simulation error, while the constraints enforce the model’s structure. This approach circumvents recursively computing the gradients of output variables over time, thus eliminating the vanishing or exploding gradient issues, although at the cost of introducing additional optimization variables.

To solve the proposed optimization problem, we leverage the *feedback linearization controlled multiplier optimization* (FL-CMO), a control-based continuous-time method for equality-constrained optimization first introduced by [Cerone et al., 2025] and later extended by [Cerone et al., 2024] and [Centorrino et al., 2025] to handle inequality constraints and non-smooth problems, respectively. More precisely, we derive and analyze a stable iterative algorithm from the FL-CMO differential equation, by using Euler integration.

This work introduces two primary contributions. First, it conducts a comprehensive theoretical analysis of the methodological approach. Specifically, the analysis concerns the relationship between the constrained and unconstrained SEM problem formulations and establishes convergence guarantees for the proposed method. We also examine the algorithm’s computational complexity and propose a strategy to mitigate its bottlenecks. Moreover, we demonstrate how to adapt the approach to handle noisy input data and state-space models.

The second contribution demonstrates the effectiveness of the proposed approach in solving several significant SI problems. The study considers four key examples. The first example shows that the proposed method outperforms standard methods for neural NIO identification on the fluid damper benchmark. In the second example, we compare our approach with state-of-the-art results on the Bouc-Wen benchmark. The third example illustrates that the proposed method enhances accuracy and reduces training time compared to state-of-the-art neural identification techniques, such as LSTM and GRU. Finally, in the fourth example, we address a realistic gray-box identification problem and compare our method with prediction-error minimization and gradient-based SEM.

The structure of the paper is as follows. Section 2

formalizes the SEM identification problem and examines the role of the vanishing gradient issue in the existing literature. Section 3 expands the proposed approach, formulating the problem as constrained optimization and developing the algorithm based on FL-CMO. Section 4 provides a theoretical analysis of the developed algorithm, establishing its relation to the standard formulation and proving its convergence. In Section 5, we leverage the problem structure and sparse QR factorization to reduce the computational complexity. Section 6 extends the proposed approach to handle errors-in-variables noise and state-space models. Finally, Section 7 presents numerical examples illustrating the effectiveness of the proposed approach, and Section 8 summarizes the findings and concludes the paper.

2 Proposed System Identification Framework

2.1 Problem Setup and Modeling

Consider an unknown dynamical system of the form

$$\begin{aligned} x_{t+1} &= f(x_t, u_t) \\ y_t &= h(x_t, u_t) \end{aligned} \quad (1)$$

where $f : \mathbb{R}^n \times \mathbb{R}^q \rightarrow \mathbb{R}^n$, $h : \mathbb{R}^n \times \mathbb{R}^q \rightarrow \mathbb{R}^p$ are unknown functions, n is the system order, $x_t \in \mathbb{R}^n$ is the state vector, and $u_t \in \mathbb{R}^q$, $y_t \in \mathbb{R}^p$ are the system’s input and output of dimensions $q \in \mathbb{N}$ and $p \in \mathbb{N}$, respectively. As discussed, for example, by [Conte et al., 1999], observability of system (1) implies the existence of the input-output description

$$y_t = \phi(y_{t-1}, \dots, y_{t-n}, u_t, \dots, u_{t-n}) \quad (2)$$

where $\phi : \underbrace{\mathbb{R}^p \times \dots \times \mathbb{R}^p}_{n \text{ times}} \times \underbrace{\mathbb{R}^q \times \dots \times \mathbb{R}^q}_{n+1 \text{ times}} \rightarrow \mathbb{R}^p$ is a suitable function depending on f and h .

This work addresses the identification of NIO models of the form

$$y_t = \mathcal{M}(y_{t-1}, \dots, y_{t-n}, u_t, \dots, u_{t-n}, \theta), \quad (3)$$

where $\mathcal{M} : \underbrace{\mathbb{R}^p \times \dots \times \mathbb{R}^p}_{n \text{ times}} \times \underbrace{\mathbb{R}^q \times \dots \times \mathbb{R}^q}_{n+1 \text{ times}} \times \mathbb{R}^{n_\theta} \rightarrow \mathbb{R}^p$ is a gray-box or black-box parametric model for ϕ and $\theta \in \mathbb{R}^{n_\theta}$ is a parameter vector of dimension $n_\theta \in \mathbb{N}$.

We assume that input-output data are available. Figure 1 illustrates the structure of the data-generating process. Specifically, The input u_t is known exactly, whereas the output measurements \tilde{y}_t are corrupted by noise according to the equation $\tilde{y}_t = y_t + \eta_t$. Here, y_t represents the noise-free output, and $\eta_t \in \mathbb{R}^p$ denotes the noise sequence.

The NIO identification problem is formulated using the SEM approach; see, for example, [Farina and Piroddi, 2010]. Accordingly, the following optimization problem is considered:

$$\underset{\zeta \in \mathbb{R}^{n_\theta + pn}}{\operatorname{argmin}} \sum_{t=1}^N \|y_t(\zeta) - \tilde{y}_t\|_W^2 + \rho(\theta) \quad (4)$$

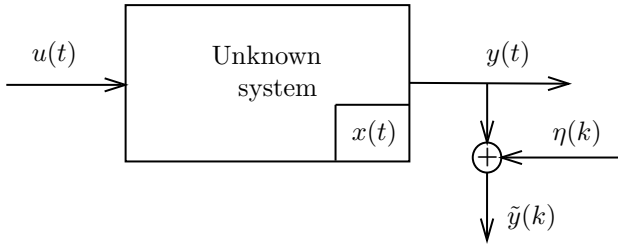


Figure 1: Block diagram of the data generation process

where $\zeta = [\theta^\top, y_1^\top, \dots, y_n^\top]^\top \in \mathbb{R}^{n_\theta + pn}$ is the vector of optimization variables, $\|\eta\|_W \doteq \sqrt{\eta^\top W \eta}$ for some positive definite matrix $W \in \mathbb{R}^{p \times p}$, $\rho : \mathbb{R}^{n_\theta} \rightarrow \mathbb{R}$ is a differentiable regularization term, and $y_t(\zeta)$ is recursively defined by

$$y_t(\zeta) = \mathcal{M}(y_{t-1}(\zeta), \dots, y_{t-n}(\zeta), u_t, \dots, u_{t-n}, \theta), \quad (5)$$

for $t = n + 1, \dots, N$.

Problem (4) generalizes the standard machine-learning formulation, as shown for example in [Salem, 2022]:

$$\operatorname{argmin}_{\theta \in \mathbb{R}^{n_\theta}} \sum_{t=1}^N \|y_t - \tilde{y}_t(\theta)\|_W^2 + \rho(\theta) \quad (6)$$

where $y_t(\theta)$ is the model output given known initial conditions. Typical assumptions include $y_t = \tilde{y}_t$ or $y_t = 0$ for $t = 1, \dots, n$ in input-output models, and $x_0 = 0$ or a random normally distributed value for state-space models. Adopting formulation (4) enables joint estimation of the initial conditions and the network parameters, leading to more accurate estimates.

2.2 Background and Related Work

The standard approach to solving Problems (4) and (6) is to apply gradient-based methods. Several techniques are available in this context. The most popular approach involves gradient-descent (GD) algorithms, such as stochastic and mini-batch GD, RM-Sprop, and Adam; see [Ruder, 2016] for a comprehensive review. Alternatively, second-order and pseudo-second-order methods are employed. Popular choices include Newton’s method, Broyden-Fletcher-Goldfarb-Shanno algorithms (see [Peng and Magoulas, 2011], [Liu et al., 2018], and [Bemporad, 2025]), and methods tailored to nonlinear least-squares problems such as the Gauss-Newton or Levenberg–Marquardt algorithms (see [Mirikitani and Nikolaev, 2009]).

All the approaches mentioned above require computing the gradients $\nabla_\theta y_t$, which recursively depend on $\nabla_\theta y_j$, for all $j = 1, \dots, t-1$. This dependence implicitly defines a dynamic relation between the gradient samples. If the dynamics is stable, the contribution to $\nabla_\theta y_t$ due to $\nabla_\theta y_k$, for $k \ll t$, is negligible (vanishing gradient). Conversely, $\nabla_\theta y_t$ is divergent if the dynamics is unstable. These phenomena are known as the vanishing and exploding gradient issues, respectively. These, discussed in [Bengio et al., 1994, Pascanu et al., 2013], cause difficulties in the learning process such as slow convergence, inaccuracy, and numerical instability.

A practical method to mitigate the exploding-gradient issue is gradient clipping, as discussed by [Ramaswamy, 2023] and the references therein. However, the vanishing-gradient problem remains unresolved in general. In black-box SI, a standard solution is to use LSTM or GRU networks, as noted by [Salem, 2022]. These networks are designed to reduce the impact of the vanishing-gradient problem, although they do not fully resolve it. Alternatively, existing gradient-free algorithms, such as that proposed in [Bas et al., 2022], are unaffected by vanishing and exploding gradients but converge slowly and require significant computational resources. [Adeoye and Bemporad, 2024] suggest formulating the identification problem as a constrained optimization task to develop a learning algorithm for recurrent neural networks using SQP. They argue that this formulation enables the development of alternative training algorithms for neural networks and provides tools to derive convergence results.

In this work, we explore a constrained optimization approach, demonstrating that it not only leads to the development of new algorithms but also ensures their resilience to vanishing-gradient issues.

3 Identification using FL-CMO algorithm

This section introduces a novel algorithm for the identification of NIO models. The method is based on the FL-CMO algorithm developed in [Cerone et al., 2025].

3.1 Constrained optimization formulation

In this section, we reformulate Problem (4) as a *constrained optimization* problem, i.e., we solve:

$$\begin{aligned} & \operatorname{argmin}_{y_1 \in \mathbb{R}^p, \dots, y_N \in \mathbb{R}^p, \theta \in \mathbb{R}^{n_\theta}} \sum_{t=1}^N \|\tilde{y}_t - y_t\|_W^2 + \rho(\theta) \\ & \text{s.t. } y_t = \mathcal{M}(y_{t-1}, \dots, y_{t-n}, u_t, \dots, u_{t-n}, \theta) \quad (7) \\ & \text{for } t = n + 1, \dots, N. \end{aligned}$$

Similar mathematical formulations can be found in [Adeoye and Bemporad, 2024], who introduce a method based on inexact SQP for training RNNs. Analogous constrained optimization problems are also formulated in the set-membership identification setting (see, e.g., [Milanese and Novara, 2004], [Milanese et al., 1996], [Cerone et al., 2014]), under the typical assumption that the noise is bounded and incorporates additional inequality constraints accordingly.

We denote $\nu \doteq n_\theta + pN$, $m \doteq N - n$, and

$$\xi = [\theta^\top, y_1^\top, \dots, y_N^\top]^\top \in \mathbb{R}^\nu, \quad (8a)$$

$$h_t(\xi) = y_{t+n} - \mathcal{M}(y_{t+n-1}, \dots, y_t, u_{t+n}, \dots, u_t, \theta), \quad t = 1, \dots, m, \quad (8b)$$

$$\mathcal{L}(\xi) = \sum_{t=1}^N \|\tilde{y}_t - y_t\|_W^2 + \rho(\theta) \quad (8c)$$

the optimization variables, constraints, and cost function of Problem (7), respectively. Let $\lambda \in \mathbb{R}^m$ be the vector of Lagrange multipliers. The first-order optimality conditions for Problem (7) are:

$$\nabla_{\xi} \mathcal{L}(\xi) + \sum_{t=1}^m \lambda_t \nabla_{\xi} h_t(\xi) = 0 \quad (9a)$$

$$h_t(\xi) = 0, \quad t = 1, \dots, m. \quad (9b)$$

Remark 1 *Conditions (9) require computing only the gradients of simple functions that do not recursively depend on other expressions. As a result, solving (9) avoids the numerical issues related to the vanishing and exploding gradient problems.*

3.2 A motivating example

To substantiate the necessity of the proposed method, we present an example illustrating how the vanishing and exploding gradient issues occur in a basic scenario and how one can address them through constrained optimization.

Consider the following first-order linear-time-invariant model:

$$y_t = \theta_1 y_{t-1} + \theta_2 u_{t-1}, \quad y_1 = 0. \quad (10)$$

The model output sample at time t is given by:

$$y_t = \sum_{k=1}^{t-1} \theta_1^{k-1} \theta_2 u_{t-k}. \quad (11)$$

Problem (6) with $W = 1$ and $\rho(\theta) = 0$ becomes

$$\min_{\theta \in \mathbb{R}^{n_{\theta}}} \mathcal{L}(\theta) = \min_{\theta \in \mathbb{R}^{n_{\theta}}} \sum_{t=2}^N \left(-\tilde{y}_t + \sum_{k=1}^{t-1} \theta_1^{k-1} \theta_2 u_{t-k} \right)^2, \quad (12)$$

and its optimal solution satisfies the optimality condition:

$$\nabla_{\theta} \mathcal{L} = 2 \sum_{t=2}^N (y_t - \tilde{y}_t) \nabla_{\theta} y_t = 0, \quad (13)$$

where

$$\nabla_{\theta} y_t = \begin{bmatrix} \frac{dy_t}{d\theta_1} \\ \frac{dy_t}{d\theta_2} \end{bmatrix} = \sum_{k=1}^{t-1} \begin{bmatrix} (k-1)\theta_1^{k-2} \theta_2 u_{t-k} \\ \theta_1^{k-1} u_{t-k} \end{bmatrix}. \quad (14)$$

In a typical gradient-descent iteration, if $|\theta_1| < 1$, the terms in the summation associated with large values of k become negligible, which can lead to numerical cancellation issues. As a result, for each time step t , only a few terms in the sum from Equation (14) significantly impact the update of the parameter estimate. On the other hand, if $|\theta_1| > 1$, the norm $\|\nabla_{\theta} y_t\|$ grows exponentially as t increases.

Using formulation (7) and according to the conditions in (9), the optimality conditions of the problem are:

$$\sum_{t=2}^N \lambda_{t-1} y_{t-1} = 0, \quad \sum_{t=2}^N \lambda_{t-1} u_{t-1} = 0 \quad (15a)$$

$$2(y_t - \tilde{y}_t) + \lambda_{t-1} - \lambda_t \theta_1 = 0, \quad \forall t = 1, \dots, N, \quad (15b)$$

$$h_{t-n} = y_t - \theta_1 y_{t-1} - \theta_2 u_t = 0, \quad \forall t = 2, \dots, N, \quad (15c)$$

where $\lambda_N = 0$.

Compared to (13), the system of equations (15) has larger dimensions: the number of variables increases from 2 to $2 + N$, and the number of equations from 2 to $2N + 1$. However, all equations are now simple bilinear functions of the unknowns x and λ , eliminating the computation of the powers of θ_1 , and thus circumventing vanishing and exploding gradient problems.

3.3 Identification algorithm based on FL-CMO

This section briefly reviews the FL-CMO dynamics introduced by [Cerone et al., 2025] and presents an iterative algorithm based on its Euler discretization.

FL-CMO addresses equality-constrained optimization problems of the form

$$\begin{aligned} \min_{\xi \in \mathbb{R}^{\nu}} f(\xi) \\ \text{s.t. } h(\xi) = 0, \end{aligned} \quad (16)$$

where $f: \mathbb{R}^{\nu} \rightarrow \mathbb{R}$, $h: \mathbb{R}^{\nu} \rightarrow \mathbb{R}^m$ are differentiable, possibly non-convex functions. The dynamics is developed using design techniques in the context of continuous-time feedback control systems, and the following equations describe the plant to be controlled:

$$\dot{\xi} = -\nabla f(\xi) - J_h(\xi) \lambda \quad (17a)$$

$$y = h(\xi). \quad (17b)$$

The Lagrange multipliers λ act as the input to the plant, while the optimization variables ξ represent the state, and the constraints define the outputs. This definition is grounded in the observation that an equilibrium point (ξ^*, λ^*) of (17) is a stationary point of (16) if and only if $h(\xi^*) = 0$; see [Cerone et al., 2025, Lemma 1]. Therefore, any feedback control system that ensures asymptotic stability and zero output regulation will inherently lead to convergence to a stationary point of (16).

Under the assumption that the Jacobian of the constraints $J_h(\xi)$ is full rank for all $\xi \in \mathbb{R}^{\nu}$, (17) has vector relative degree $r = [1, \dots, 1]^T \in \mathbb{R}^m$ [Cerone et al., 2025, Lemma 2], and therefore the non-interacting control problem defined in the context of feedback linearization admits a solution, as shown in [Isidori, 1995] and [Khalil, 2002]. Applying the technique of output-feedback linearization controller design, we obtain the controller:

$$\lambda = (J_h(\xi) J_h^T(\xi))^{-1} (J_h(\xi) \nabla_{\xi} f(\xi) + v) \quad (18a)$$

$$v = Ky, K > 0. \quad (18b)$$

The continuous-time closed-loop system (17)-(18) defines the FL-CMO dynamics, which locally converges to a solution of the constrained optimization problem (16). We refer the reader to Section 4.2 for a detailed convergence analysis.

We integrate the differential equations describing the FL-CMO dynamics using the Euler method; see [Wanner and Hairer, 1996] and [Sundnes, 2024]. Algorithm 1 illustrates the resulting procedure.

Algorithm 1 Identification algorithm based on FL-CMO and Euler discretization

Require: $\xi_0, \epsilon_f, \epsilon_h, K, \tau$

$k \leftarrow 0$

while $\|\delta_\xi\|_2 \geq \epsilon_f$ or $\|h(\xi_k)\|_2 \geq \epsilon_h$ **do**

$J = J_h(\xi_k)$

$\delta_\xi = -\nabla f(\xi_k) - J^\top (JJ^\top)^{-1} (J\nabla f(\xi_k) + Kh(\xi_k))$

$\xi_{k+1} = \xi_k + \tau\delta_\xi$

$k \leftarrow k + 1$

end while

The computation of the Jacobian $J = J_h(\xi_k)$ of the constraints h can be performed using automatic differentiation, see, e.g., [Baydin et al., 2018], or closed-form expressions derived through tensor calculus rules, see, e.g., [Laue et al., 2018]. Both approaches efficiently perform this computation by leveraging parallelization.

4 Theoretical Analysis

This section analyzes the theoretical properties of Algorithm 1.

4.1 Relation with the unconstrained formulation

By construction, the constrained formulation (7) and the unconstrained one (4) share the same global optimal solutions. However, local solutions may differ between the two. The following theorem establishes a connection between the local solutions of (7) and those of (4).

Theorem 1 *If a point $[\theta^\top, y_1^\top, \dots, y_N^\top]^\top \in \mathbb{R}^{n_\theta + pN}$ satisfies the first-order optimality conditions of Problem (7), the point $[\theta^\top, y_1^\top, \dots, y_n^\top]^\top \in \mathbb{R}^{n_\theta + pn}$ is a stationary point of Problem (4).*

Proof. We denote $z = [\theta^\top, y_1^\top, \dots, y_n^\top]^\top \in \mathbb{R}^{n_\theta + pn}$, and $w = [y_{n+1}^\top, \dots, y_N^\top]^\top \in \mathbb{R}^m$, where $m = p(N - n)$. Let $h(z, w)$ denote the constraints of (7) and $J_h(z, w) = [J_{h,z}, J_{h,w}]$ its Jacobian. By construction, $J_{h,w} \in \mathbb{R}^{m \times m}$ is block-triangular with all the blocks on the main diagonal being full rank, making it invertible. Denote $G(w) = \sum_{t=n+1}^N \|y_t - \tilde{y}_t\|_W^2$ and $R(z) = \sum_{t=1}^n \|y_t - \tilde{y}_t\|_W^2 + \rho(\theta)$. The first-order optimality conditions are given by

$$\nabla_z R + J_{h,z}^\top \lambda = 0 \quad (19a)$$

$$\nabla_w G + J_{h,w}^\top \lambda = 0. \quad (19b)$$

From (19b) we obtain

$$\lambda = - (J_{h,w}^\top)^{-1} \nabla_w G \quad (20)$$

and substituting (20) into (19a) we obtain

$$\nabla_z R - J_{h,z}^\top (J_{h,w}^\top)^{-1} \nabla_w G = 0. \quad (21)$$

By applying the Implicit Function Theorem, and noting that $h(z, w) = 0$ and $J_{h,w}$ is invertible, there exists a function $\gamma : \mathbb{R}^{n_\theta + pn} \rightarrow \mathbb{R}^m$ such that $w = \gamma(z)$. Moreover, the Jacobian $J_{\gamma,z}$ of γ satisfies

$$J_{\gamma,z} = -J_{h,w}^{-1} J_{h,z}. \quad (22)$$

We now consider Problem (4), for which the stationary points satisfy

$$\nabla_z G(\gamma(z)) + \nabla_z R(z) = 0. \quad (23)$$

By applying the chain rule and Equation (22), we derive the following expression:

$$\begin{aligned} \nabla_z R(z) + \nabla_z G(\gamma(z)) &= \\ &= \nabla_z R + [\nabla_{\gamma(z)} G^\top J_{\gamma,z}]^\top = \\ &= \nabla_z R - [\nabla_w G^\top J_{h,w}^{-1} J_{h,z}]^\top = \\ &= \nabla_z R - J_{h,z}^\top (J_{h,w}^\top)^{-1} \nabla_w G, \end{aligned} \quad (24)$$

which equals zero by (21). \square

Theorem 1 emphasizes that solving (7) instead of (4) does not introduce any additional local solutions.

4.2 Analysis of local convergence

In the following theorem, we analyze the convergence of Algorithm 1.

Theorem 2 (Convergence of Algorithm 1) *Any point (ξ^*, λ^*) satisfying the second-order sufficient conditions of Problem (7) is a locally asymptotically stable equilibrium of Algorithm 1 if τ is sufficiently small.*

Proof. First, we note that the assumptions required to apply the FL-CMO method hold:

- By construction, Problem (7) is characterized by $m < \nu$, meaning that the number of optimization variables is larger than the number of constraints.
- $\text{rank}(J_h(\xi)) = m$ for any $\xi \in \mathbb{R}^\nu$. This condition holds because $J_h(\xi)$ consistently maintains full rank, as demonstrated by the argument used for the $J_{h,w}$ submatrix in the proof of Theorem 1.

Under these conditions, Theorem 4 in [Cerone et al., 2025] is applicable. Consequently, any point (ξ^*, λ^*) satisfying the second-order sufficient conditions of Problem (7) is a locally asymptotically stable equilibrium point of the dynamics (17)-(18). Finally, the argument remains valid after the Euler discretization because it preserves the equilibrium points and their stability properties if τ is sufficiently small; see, e.g., [Wanner and Hairer, 1996]. \square

The assumption that τ must be sufficiently small to ensure stability closely parallels the requirement for a small learning rate in standard gradient-based optimization for unconstrained problems in machine learning. As in those settings, the value of τ must be chosen carefully: if it is too large, the algorithm diverges; if it is too small, convergence becomes slow.

5 Analysis of the computational complexity

The primary computational cost of Algorithm 1 arises from computing:

$$\sigma \doteq (J_h(\xi_k) J_h^\top(\xi_k))^{-1} (J_h(\xi_k) \nabla f(\xi_k) + Kh(\xi_k)). \quad (25)$$

This section demonstrates how the problem's structure can be leveraged to reduce the computational complexity related to the main computational bottleneck of Algorithm 1: the inversion of the matrix $(J_h(\xi_k)J_h^\top(\xi_k))$.

Suppose that we use a standard decomposition method to compute the triangular Cholesky factor R of $J_h(\xi_k)J_h^\top(\xi_k)$. The computational complexity of such an operation is $O(m^3)$. See [Stewart, 1998] for a detailed analysis of the computational complexity of these algorithms. In the following, we present a method for solving the linear system (25) that exploits the sparsity of $J_h(\xi_k)$ to reduce the overall computational effort to $O(m^2)$. Specifically, the method proceeds as follows:

1. Perform the Q-free QR decomposition of $J_h^\top(\xi_k)$, i.e., obtain the upper triangular factor $R \in \mathbb{R}^{m \times m}$, where an orthogonal matrix Q satisfies $J_h^\top(\xi_k) = QR$. This method employs the sparse Householder algorithm described in [Davis, 2011]. By applying the QR factorization, we obtain $J_h(\xi_k)J_h^\top(\xi_k) = R^\top Q^\top QR = R^\top R$, which makes R^\top a Cholesky factor of $J_h(\xi_k)J_h^\top(\xi_k)$.
2. Apply forward and backward substitution to compute the solution of the linear system.

Proposition 1 *Using the sparse Householder algorithm, the computational complexity of a generic iteration of Algorithm 1 is $O(m^2)$.*

Proof. We calculate the operations required for the Householder algorithm that exploits sparsity by avoiding multiplications involving zeros. Table 1 reports the number of floating-point operations (FLOPs) for each step of the Householder algorithm applied to the matrix $X = J_h^\top(\xi_k)$, comparing the dense and sparse cases.

To analyze the first instruction of the loop, we examine the function $[u, \mu] = \text{housegen}(w)$. This function performs the Householder reflection of its argument by computing u such that $(I - uu^\top)w = \pm \|w\|_2 e_1$, where e_1 is the first vector of the standard Euclidean basis. For additional details, refer to [Stewart, 1998]. The *house-*

Algorithm 2 The *housegen* function

```

 $u = w, \quad \mu = \|w\|_2$ 
if  $\nu = 0$  then
     $u_1 = \sqrt{2}, \quad \text{return}$ 
end if
 $u = w/\mu$ 
if  $u_1 \geq 0$  then
     $u_1 = u_1 + 1, \quad \mu = -\mu$ 
else
     $u_1 = u_1 - 1$ 
end if
 $u = u/\sqrt{|u_1|}$ 

```

gen function is defined according to Algorithm 2. The computational cost of *housegen* is primarily driven by the calculation of $\mu = \|w\|_2$, $u = w/\mu$, and $u = u/\sqrt{|u_1|}$. Each of these operations involves χ FLOP products, where χ is the cardinality of w . Consequently, since ξ_k is constructed from the k -th to the n -th element of

X , this step requires $3(\nu - k + 1)$ FLOPs in the dense case and $3\chi(k)$ FLOPs when exploiting sparsity. Based on the structure of $X = J_h^\top(\xi_k)$, $\chi(k)$ is given by

$$\chi(k) = \begin{cases} n_\theta - k + 1 + p(1 + n) & \text{if } k \leq n_\theta \\ p(1 + n) & \text{if } k > n_\theta. \end{cases} \quad (26)$$

Computing the product $U_{k:\nu, k}^\top X_{k:\nu, k+1:m}$ in the dense case requires $(\nu - k + 1)(m - k)$ multiplications. In the sparse case, however, $U_{k:\nu, k}$ exhibits the same sparsity pattern as ξ_k , except for its first element, which consistently provides no contribution to the product. By leveraging this sparsity, the number of required products drops to

$$\psi(k) = \begin{cases} \psi_1(k) & \text{if } k \leq n_\theta \\ \psi_2(k) & \text{if } k > n_\theta, \end{cases} \quad (27)$$

where, for $i = (k \bmod p) + 1$, we obtain

$$\begin{aligned} \psi_2(k) &= (p - i)p(n + 1) + np^2 + \dots + 2p^2 + p^2 \\ &= (p - i)p(n + 1) + \sum_{z=1}^n zp^2, \end{aligned} \quad (28)$$

$$\psi_1(k) = (n_\theta - k + 1)(m - k) + \psi_2(k). \quad (29)$$

Equation (28) follows from the observation that the number of coinciding nonzero indices decreases by p every p columns. Similarly, Equation (29) is obtained using the same procedure while also accounting for the contributions of products involving the first $(n_\theta - k + 1)$ elements of $U_{k:\nu, k}^\top$.

We now compute $\zeta(k)$ representing the number of FLOPs required to calculate the product $U_{k:\nu, k}v$, where $U_{k:\nu, k} \in \mathbb{R}^{\nu-k+1}$ is a sparse vector with cardinality

$$\chi_1(k) = \begin{cases} \chi(k) & \text{if } k \leq n_\theta \\ \chi(k) + 1 & \text{if } k > n_\theta \end{cases} \quad (30)$$

and $v \in \mathbb{R}^{1, m-k}$ is possibly dense. Accordingly, the result is an $(\nu - k + 1) \times (m - k)$ matrix in which all rows corresponding to zero elements of $U_{k:\nu, k}$ are zero. As a result, the dense case requires $(\nu - k + 1)(m - k)$ FLOPs, whereas the sparse case requires

$$\zeta(k) = (m - k)\chi_1(k) \text{ FLOPs.} \quad (31)$$

To conclude the proof, we demonstrate the existence of constants $M > 0$ and $m_0 > 0$ such that for all $m > m_0$:

$$\left| \sum_{k=1}^m 3\chi(k) + \psi(k) + \zeta(k) \right| \leq Mm^2. \quad (32)$$

Let us evaluate each term of the sum:

$$\begin{aligned} \sum_{k=1}^m 3\chi(k) &= 3 \sum_{k=1}^{n_\theta} (n_\theta - k + 1 + p(1 + n)) + \\ &+ 3 \sum_{k=n_\theta+1}^m p(1 + n) = 3m(1 + n)p + \frac{3}{2}(n_\theta^2 + n_\theta) \end{aligned} \quad (33)$$

Table 1: FLOPs count for each instruction of the Housholder algorithm.

Instruction	Iterations	FLOPs - dense	FLOPs - sparse
$U = 0_{\nu \times m}, R = 0_{m \times m}$	1	-	-
for $k = 1, \dots, m$			
$U_{k:\nu, k}, R_{k, k} = \text{housegen}(X_{k:\nu, \nu})$	m	$3(\nu - k + 1)$	$3\chi(k)$
$v = U_{k:\nu, k}^\top X_{k:\nu, k+1:m}$	m	$(\nu - k + 1)(m - k)$	$\psi(k)$
$X_{k:\nu, k+1:m} = X_{k:\nu, k+1:m} - U_{k:\nu, k} v$	m	$(\nu - k + 1)(m - k)$	$\zeta(k)$
$R_{k, k+1:m} = X_{k, k+1:m}$	m	-	-
end for			

$$\begin{aligned} \sum_{k=1}^m \psi(k) &= \sum_{k=1}^{n_\theta} \psi_1(k) + \sum_{k=n_\theta+1}^m \psi_2(k) \\ &= \sum_{k=1}^{n_\theta} (n_\theta - k + 1)(m - k) + \sum_{k=1}^m \psi_2(k) \end{aligned} \quad (34)$$

$$\begin{aligned} \sum_{k=1}^m \zeta(k) &= \sum_{k=1}^{n_\theta} (n_\theta - k + 1 + p(n + 1))(m - k) + \\ &+ \sum_{k=n_\theta+1}^m (p(n + 1) + 1)(m - k) = \\ &= \sum_{k=1}^{n_\theta} (n_\theta - k)(m - k) + \sum_{k=1}^m (p(n + 1) + 1)(m - k) = \\ &= \frac{m}{2}(n_\theta^2 - n_\theta) - \frac{n_\theta}{6}(n_\theta^2 - 1) + \frac{m^2 - m}{2}(p(n + 1) + 1) \\ &= \frac{m^2}{2}(p(n + 1) + 1) + \\ &+ \frac{m}{2}(n_\theta^2 - n_\theta - p(n + 1) - 1) - \frac{n_\theta}{6}(n_\theta^2 - 1). \end{aligned} \quad (35)$$

Let us expand individually the two terms in equation (34) to analyze their contributions.

$$\begin{aligned} \sum_{k=1}^{n_\theta} (n_\theta - k + 1)(m - k) &= \\ &= \frac{m}{2}(n_\theta^2 - n_\theta) - \frac{n_\theta}{6}(n_\theta^2 + 3n_\theta + 2) \end{aligned} \quad (36)$$

$$\begin{aligned} \sum_{k=1}^m \psi_2(k) &= \sum_{k=1}^m \left((p - i)(n + 1)p + \sum_{z=1}^n p^2 z \right) = \\ &= \sum_{j=1}^{m/p} \sum_{i=1}^p \left((p - i)(n + 1)p + \sum_{z=1}^n p^2 z \right) = \\ &= \frac{m}{p} \left(p^3(n + 1) - \frac{1}{2}(n + 1)p^2(p + 1) \right) + \\ &+ \frac{1}{2}mp^2n(n + 1) = \frac{1}{2}mp(n + 1)(p + pn - 1) \end{aligned} \quad (37)$$

From the above equations, we observe that (35) dominates (33) and (34). By choosing M in equation (32) to be greater than $\frac{1}{2} + \frac{1}{2}p(n + 1)$, the result follows. \square

Remark 2 The sparsity of $J_h(\xi_k)$ can also be exploited when computing the matrix-vector products $J_h(\xi_k)\nabla f(\xi_k)$ and $J_h^\top(\xi_k)\sigma$. Table 2 presents the FLOP count for both dense and sparse algorithms.

We evaluate the practical implications of the achieved reduction in computational complexity proven in Proposition 1 through a series of numerical experiments. We

Table 2: FLOP count for matrix-vector multiplications

Instruction	FLOPs - dense	FLOPs - sparse
$J_h(\xi_k)\nabla f(\xi_k)$	$m(n_\theta + N)$	$m(n_\theta + pn)$
$J_h^\top(\xi_k)\sigma$	m^2	$m(n_\theta + pn)$

construct a synthetic problem with $p = n = 2$ and measure the time required to perform a single iteration of Algorithm 1 across varying dataset dimensions. The results demonstrate relative speedups of $1.6\times$, $3.7\times$, and $5.7\times$ for $N = 10^3$, $N = 5 \cdot 10^3$, and $N = 10^4$, respectively.

Compared to the inexact SQP method proposed by [Adeoye and Bemporad, 2024], we note that the size of the matrix requiring QR factorization decreases from $(\nu + m) \times (\nu + m)$ to $m \times (\nu + m)$. As a consequence, we conclude that Algorithm 1 benefits from reduced computational complexity compared to the inexact SQP method by [Adeoye and Bemporad, 2024]. Moreover, the iterations are exact, significantly simplifying the analysis.

6 Extensions to error-in-variables and state-space models

This section demonstrates the application of the constrained-optimization reformulation and Algorithm 1 to identification problems with a structure differing from that considered in Section 3.

6.1 Errors-in-variables models

The constrained optimization approach generalizes to scenarios in which both the input and output data are corrupted by noise. In this case, the available dataset is $\{\tilde{u}_t, \tilde{y}_t\}$, for $t = 1, \dots, N$, where $\tilde{u}_t = u_t + \epsilon_t$, $\tilde{y}_t = y_t + \eta_t$. Here, $\epsilon_t \in \mathbb{R}^q$, $\eta_t \in \mathbb{R}^p$ denote the noise components. This setting is commonly referred to as the errors-in-variables (EIV) model.

We formalize this task by solving the following opti-

mization problem

$$\begin{aligned}
& \underset{\theta \in \mathbb{R}^{n_\theta}, u_1 \in \mathbb{R}^q, \dots, u_N \in \mathbb{R}^p}{\operatorname{argmin}} \sum_{t=1}^N \|y_t - \tilde{y}_t\|_{W_y}^2 + \\
& + \sum_{t=1}^N \|u_t - \tilde{u}_t\|_{W_u}^2 + \rho(\theta) \\
& \text{s.t. } y_t = \mathcal{M}(y_{t-1}, \dots, y_{t-n}, u_t, \dots, u_{t-n}, \theta) \\
& \quad \text{for } t = n+1, \dots, N.
\end{aligned} \tag{38}$$

where $W_y, W_u \succ 0$ are weighting matrices. When output noise is expected to exceed input noise, $W_u \succ W_y$. As W_u approaches infinity ($W_u \rightarrow \infty$), \tilde{u} becomes equivalent to u ($\tilde{u} = u$), recovering the standard output error problem.

The theoretical analysis presented in Section 4 also applies to this case, whereas the considerations on computational complexity are different from those in Section 5 due to the distinct sparsity of the problem. Compared to Problem (7), introduced in Section 3 for the output-error case, the number of optimization variables rises, while the number of constraints remains unchanged. Consequently, the dimensions of the linear system (25) remain unchanged. Furthermore, J is still sparse, and numerical experiments demonstrate that the proposed QR decomposition offers computational benefits.

6.2 State-space models

State-space models are a widely used description for dynamical systems owing to their versatility, as they encompass linear systems, gray-box models, recurrent neural networks, and neural state-space models. In this section, we propose a constrained optimization formulation of the SEM problem for state-space models.

Given a dynamical model for system (1) defined by

$$\begin{aligned}
x_{t+1} &= \mathcal{M}_1(x_t, u_t, \theta), \\
y_t &= \mathcal{M}_2(x_t, u_t, \theta)
\end{aligned} \tag{39}$$

where $\mathcal{M}_1 : \mathbb{R}^n \times \mathbb{R}^q \times \mathbb{R}^{n_\theta} \rightarrow \mathbb{R}^n$ and $\mathcal{M}_2 : \mathbb{R}^n \times \mathbb{R}^q \times \mathbb{R}^{n_\theta} \rightarrow \mathbb{R}^p$, we can recast its SEM identification as the following constrained optimization problem:

$$\begin{aligned}
& \underset{\theta \in \mathbb{R}^{n_\theta}, x_1 \in \mathbb{R}^n, \dots, x_N \in \mathbb{R}^n}{\operatorname{argmin}} \sum_{t=1}^N (\mathcal{M}_2(x_t, u_t, \theta) - \tilde{y}_t)_2^2 + \rho(\theta) \\
& \text{s.t. } x_{t+1} = \mathcal{M}_1(x_t, u_t, \theta), \quad t = 1, \dots, N-1.
\end{aligned} \tag{40}$$

Problem (40) involves $n(N-1)$ optimization variables. Since, for many practical cases $p < n$, i.e., there are fewer outputs than states, this value is greater than the NIO counterpart $p(N-n)$. For this reason, input-output models are computationally preferable when using a constrained optimization approach. Furthermore, as shown in the numerical example of Section 7.3, input-output models are less prone to overfitting than state-space models.

7 Numerical examples

This section presents numerical examples demonstrating the effectiveness of the proposed method. The examples

compare the proposed approach with established alternatives on widely used SI benchmarks. MATLAB code and generated data for all examples are available on the GitHub page: https://github.com/SimonePirrera97/SEM_SysID_with_FLCMO.

In the following examples, we consider both gray-box and black-box identification problems. For the black-box case, we employ the well-established approach of using neural networks, owing to their ability to approximate any continuous function. Specifically, in all black-box examples, we adopt neural NIO models, i.e., models of the form (3) where \mathcal{M} is implemented by a neural network. Following the notation introduced by [Sjöberg et al., 1994], we denote the neural NIO model as a nonlinear neural output error (NNOE) model when its training is performed through minimization of the simulation error, and as a nonlinear neural auto-regressive exogenous input (NNARX) model when it is trained by prediction-error minimization.

In the first example, we compare different neural NIO approaches. The second example validates the effectiveness of the proposed algorithm on a well-established system identification benchmark. The third example compares NNOE training using the proposed method with identification based on recurrent neural networks. Finally, the fourth example addresses gray-box identification of a magnetic levitation system.

The validation metrics adopted here include the root-mean-squared error (RMSE) and the best-fit rate (BFR), defined as:

$$\text{RMSE} \doteq \sqrt{\frac{1}{N} \|\hat{y} - y\|_2^2}, \quad \text{BFR} \doteq \left(1 - \frac{\|y - \hat{y}\|}{\|y - m_y\|}\right), \tag{41}$$

where y denotes the measured validation output, \hat{y} the simulated output, and m_y the sample mean of y .

Each of the following examples will consider a different value for the parameter K , to highlight the algorithm's robustness to its selection. The value of τ is selected via a trial-and-error procedure to ensure stability of the learning dynamics.

7.1 Fluid Damper Benchmark

This subsection examines the magneto-rheological fluid damper problem from [Wang et al., 2009]. The problem considers magneto-rheological fluid dampers, which are devices used to suppress mechanical vibrations. These dampers contain fluids whose viscosity varies in response to a control signal. The benchmark dataset was obtained by attaching the test damper to a shaker table that generates realistic vibrations. Experimental data from these tests, comprising 2000 data points for training and 1499 data points for testing, are available in MATLAB's System Identification Toolbox.

This subsection evaluates the proposed FL-CMO-based algorithm against leading alternatives for neural NIO modeling in SI, namely NNARX identification via backpropagation and NNOE training with the Levenberg-Marquardt algorithm.

We select a single-layer network with a dynamical order $n = 4$ and 6 neurons. The identification process

involved the following methods:

1. NNARX: We trained the network using Adam stochastic gradient descent with a batch size of 32. The training algorithm was implemented in Python using TensorFlow’s Keras package, see [Chollet et al., 2015], with the network trained for 2000 epochs.
2. NNOE with Levenberg-Marquardt: We used the *nnoe* function from the NNSYD MATLAB toolbox, see [Nørgård et al., 1996], which applies the Levenberg-Marquardt algorithm. The gradient and criterion-improvement tolerances were set to 10^{-12} , while the maximum number of iterations was set to 10^5 .
3. NNOE with the proposed FL-CMO algorithm: We set the parameters to $\tau = 2 \cdot 10^{-3}$ and $K = 1$, with a maximum of 1000 iterations and regularization $\rho(\theta) = 10^{-3} \|\theta\|_2^2$.

We repeat the identification process 10 times, with different, normally distributed, initializations of the optimization variables. Table 3 reports the mean value and standard deviation of the training times (measured in seconds) and validation BFRs across all runs for the different algorithms. The results indicate the FL-CMO algorithm requires lower computational effort compared to Adam while delivering superior performance. In contrast, the Levenberg-Marquardt algorithm significantly reduces computational effort; however, it is less reliable due to the vanishing gradient issue, resulting in poorer average performance.

The obtained results are consistent with or improve upon those reported in Table I of [Bemporad, 2022], which are based on the same dataset. Specifically, standard BPTT training with the Adam optimizer achieves a validation BFR of 85.5% for both RNN and LSTM models, while the extended Kalman filter approach proposed in [Bemporad, 2022] yields BFRs of 89.78% and 88.97% for RNN and LSTM, respectively.

7.2 Bouc-Wen system benchmark

This section considers the Bouc-Wen model, which is described by the dynamics:

$$\begin{aligned} m_L \ddot{y}(t) + c_L \dot{y}(t) + k_L y(t) + z(t) &= u(t) \\ \dot{z}(t) &= \alpha \dot{y}(t) - \beta (\gamma |\dot{y}(t)| |z(t)|^{\nu-1} z(t) + \delta \dot{y}(t) |z(t)|^\nu), \end{aligned} \quad (42)$$

where $m_L, k_L, c_L, \alpha, \beta, \gamma, \nu, \delta$ are real scalars. This model is extensively used to characterize mechanical hysteretic effects. The problem of performing its identification belongs to the benchmarks considered during the annual Nonlinear System Identification Benchmarks workshop. For a comprehensive description of the problem, refer to [Noel and Schoukens, 2016].

A total of 5000 data pairs for training and 5000 data pairs for validation were generated using a multisine input signal, adhering to the provided MATLAB function with its default settings. Training and validation output data were corrupted by additive Gaus-

sian noise with a variance of $8 \times 10^{-3} \text{ mm}^2$. For testing, the data provided in the files "uval_multisine.mat" and "yval_multisine.mat" were used, which include 8192 data pairs.

We train NNOE networks with a dynamical order $n = 3$ and two layers, varying the number of neurons from 5 to 10. Training is performed using Algorithm 1, with $\tau = 2 \cdot 10^{-3}$, $K = 10$, $\epsilon_f, \epsilon_h = 10^{-4}$ and regularization $\rho(\theta) = 10^{-3} \|\theta\|_2^2$. Among the trained networks, the model containing 8 neurons was selected, as it achieved the highest validation accuracy with a BFR index of 87.38%. The network has 145 parameters, and its training requires 3000 iterations of Algorithm 1, corresponding to 3521 s of computations. The achieved BFR on the provided test set is 95.01%, demonstrating the model’s generalization capabilities.

Table 4 presents the validation RMSE of the trained model and compares it with previously reported results on this benchmark. It is noteworthy that the obtained NNOE model demonstrates superior accuracy compared to the method by [Belz et al., 2017] and accuracy comparable to those by [Forgione and Piga, 2021], using only 5000 training data points rather than 40960, emphasizing the data efficiency of the NNOE model. This performance can be attributed to the NNOE model’s reduced parameterization, which enables effective learning from smaller datasets and mitigates the risk of convergence to poor local minima. In contrast, accuracy remains lower compared that obtained with the technique introduced by [Esfahani et al., 2017], which is designed specifically for hysteretic systems.

7.3 MIMO Wiener-Hammerstein system

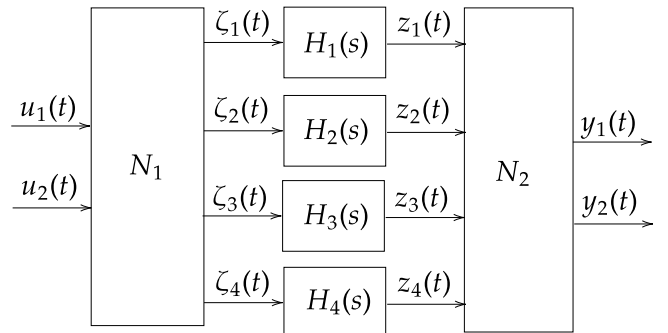


Figure 2: MIMO Wiener-Hammerstein system diagram.

In this subsection, we address the identification of the Wiener-Hammerstein system shown in Figure 2, which features two inputs and two outputs. The problem is challenging because the overall behavior is governed by the interplay between linear dynamic blocks and nonlinear components, leading to complex system responses. The input nonlinear block is described by

$$\zeta_1 = 0.2u_1u_2 - u_1 - u_2 - 0.04u_2^2(u_2 + u_1), \quad (43a)$$

$$\zeta_2 = u_1 + u_2, \quad \zeta_3 = 2u_2 - 1.3\zeta_1, \quad \zeta_4 = u_1, \quad (43b)$$

Table 3: Example 1. Comparison of NNARX (Adam) and NNOE (FL-CMO and Levenberg-Marquardt) identification methods.

	training time	BFR
NNOE using FL-CMO	106.68 (1.17)	88.28 (1.29)
NNOE using Levenberg-Marquardt)	0.32 (0.097)	66.66 (27.14)
NNARX using Adam	176.22 (32.27)	68.14 (23.32)

Table 4: Example 2: Comparison of several methods on the Bouc-Wen system benchmark.

Method	RMSE
[Esfahani et al., 2017]	1.87×10^{-5} mm
[Belz et al., 2017]	16.3×10^{-5} mm
[Forgione and Piga, 2021]	4.52×10^{-5} mm
NNOE trained by FL-CMO	3.33×10^{-5} mm

the linear blocks by

$$H_1(s) = \frac{16}{s^2 + 40s + 130}, \quad (43c)$$

$$H_2(s) = \frac{80}{s^3 + 31s^2 + 340s + 2730}, \quad (43d)$$

$$H_3(s) = \frac{30}{s + 10}, \quad H_4(s) = \frac{-10}{s^2 + 6s + 80}, \quad (43e)$$

and output nonlinear block by

$$y_1 = 7.5z_4z_1 - 51z_2 + 1.02z_4^2z_2 - 9z_1^3 \quad (43f)$$

$$y_2 = 2.7z_2z_3 - 0.729z_4z_2^2. \quad (43g)$$

We generate a training dataset by simulating the system for 35 seconds and sampling the obtained signals with period $T_s = 0.01$ s, yielding $N = 3500$ training samples. Similarly, we generate a test dataset of 5000 samples. In both cases, the input signal is a staircase signal with stair length $T_{\text{stair}} = 100T_s$ and normally distributed amplitudes with unitary variance.

We train several NNOE models with dynamical order $n = 3$ and different neural network structures using the proposed Algorithm 1 with parameters $\tau = 0.01, K = 100, \epsilon_f = \epsilon_h = 10^{-3}$, and the maximum of 500 iterations. We compare the results obtained using our method with those provided by training LSTM, GRU, and NNARX networks with various architectures. Training of LSTM and GRU is performed using the BPTT algorithm, while the NNARX networks are trained using standard backpropagation (Adam algorithm). To assess model quality, we evaluate the test RMSE and BFR. Table 5 summarizes the numerical results concerning training time and accuracy, and marks in green the top-performing models within each class: NNOE(2,5), with two layers of five neurons each; LSTM(2,2), with two layers of two cells; and GRU(1,5), including a single layer of five cells. Figure 3 presents the validation outputs of these models.

The results reported in Table 5 indicate that the NNARX, LSTM, and GRU models require longer training times and yield lower prediction accuracy than the NNOE model. In particular, the simulation performance of NNARX is significantly worse. This can be attributed to NNARX training relying on PEM, whereas the other

models employ SEM. At the same time, the superior performance of NNOE with respect to LSTM and GRU stems from its higher data efficiency and the resilience of its training process to vanishing gradient issues.

Concerning computational effort, the columns time/iter and time/epoch in Table 5 report the average computation time per iteration of Algorithm 1 and per epoch of BPTT, respectively. From these results, we observe that a single iteration of Algorithm 1 is more computationally demanding than one BPTT epoch for LSTM and GRU training. However, training NNOEs with Algorithm 1 requires significantly fewer iterations overall, resulting in a lower total training time. This improvement is primarily due to the absence of vanishing gradient issues.

7.4 Magnetic levitation system gray-box identification

We analyze the magnetic levitation system described by the continuous-time model

$$\ddot{z} = g - \frac{k_m i^2 + k_0}{mz^2}, \quad (44)$$

where z denotes the distance between the magnet and the ball, m is the mass of the ball, g denotes the gravitational acceleration, and k_m and k_0 are constants determined by the magnet's characteristics. The objective of the identification procedure is to estimate k_m and k_0 , with $m = 24.197$ g and $g = 9.81$ m/s² treated as known constants.

We simulate the differential equation (44) and collect $N = 200$ input-output data points using a sampling rate of $T_s = 10$ ms. The output data is subsequently corrupted by additive measurement noise uniformly distributed within the interval $[-5, 5]$ mm.

We discretize the dynamic system equation using Euler's method, resulting in the following model

$$m z_{t-2}^2 \left(\frac{z_t - 2z_{t-1} + z_{t-2}}{T_s^2} - g \right) + k_m i_{t-2}^2 + k_0 = 0. \quad (45)$$

According to the proposed approach, we evaluate the Jacobian of the constraints defined in Equation (45). Specifically, the computation requires determining the partial derivatives:

$$\frac{\partial h_t}{\partial k_m} = i_{t-2}^2, \quad \frac{\partial h_t}{\partial z_t} = \frac{m}{T_s^2} z_{t-2}^2, \quad (46a)$$

$$\frac{\partial h_t}{\partial z_{t-1}} = -\frac{2m}{T_s^2} z_{t-2}^2, \quad \frac{\partial h_t}{\partial k_0} = 1, \quad (46b)$$

$$\frac{\partial h_t}{\partial z_{t-2}} = \frac{m}{T_s^2} z_{t-2} (2z_t - 4z_{t-1} + 3z_{t-2}) - 2mgz_{t-2}. \quad (46c)$$

Table 5: Example 3: Comparison of several networks.

NNOE network				NNOE Training: FL-CMO algorithm (CPU)					NNOE Validation			
order	layers	neuron/layer	# param.	RMSE y_1	RMSE y_2	iterations	time	time/iter	RMSE y_1	RMSE y_2	BFR y_1	BFR y_2
3	1	5	87	0.4667	0.3141	320	514.19	1.607	0.2816	0.2670	86.03%	83.00%
3	1	8	138	0.4411	0.2979	285	633.59	2.223	0.4557	0.3528	77.39%	77.54%
3	1	10	172	0.3535	0.0295	500	817.81	1.636	0.1133	0.0864	94.38%	94.50%
3	1	15	257	0.3532	0.0252	420	703.28	1.674	0.1145	0.0925	94.32%	94.11%
3	2	3	65	0.3880	0.1733	300	474.93	1.583	0.1622	0.2078	91.95%	86.77%
3	2	5	117	0.3550	0.0728	360	585.42	1.626	0.0994	0.1071	95.07%	93.18%
3	2	7	177	0.4979	0.2764	480	777.75	1.620	0.2942	0.1718	85.41%	89.06%
3	2	10	282	0.3541	0.0255	500	826.19	1.652	0.1188	0.1097	94.11%	93.02%
3	3	3	77	0.4049	0.1898	260	453.32	1.744	0.1494	0.1958	92.59%	87.54%
3	3	5	147	0.4247	0.2683	180	438.12	2.434	0.2694	0.2975	86.64%	81.06%
3	3	7	233	0.6969	0.7338	140	244.47	1.746	0.2452	0.2378	87.84%	84.86%

LSTM network				LSTM Training: Adam BPTT algorithm (GPU)					LSTM Validation			
order	layers	units/layer	# param.	RMSE y_1	RMSE y_2	epochs	time	time/epoch	RMSE y_1	RMSE y_2	BFR y_1	BFR y_2
4	1	2	46	0.5475	0.4164	12000	841.05	0.0701	0.6236	0.7680	69.06%	51.11%
6	1	3	80	0.4142	0.3207	12000	821.17	0.0684	0.5876	0.6221	70.85%	60.40%
8	1	4	122	0.2371	0.1841	12000	1036.00	0.0863	0.4236	0.2769	78.99%	82.37%
10	1	5	172	0.0793	0.0790	12000	827.54	0.0690	0.3811	0.2150	81.09%	86.31%
14	1	7	296	0.0545	0.0505	12000	826.17	0.0688	0.3606	0.2628	82.11%	83.27%
8	2	2	86	0.2747	0.2142	12000	1690.19	0.1408	0.3254	0.2512	83.86%	84.00%
12	2	3	164	0.2131	0.1636	12000	3061.88	0.2552	0.3858	0.4607	80.86%	70.67%
16	2	4	266	0.1781	0.1543	12000	2879.37	0.2399	0.8467	0.4391	58.00%	72.04%
20	2	5	392	0.1867	0.1390	12000	2392.98	0.1994	0.8459	0.7204	58.04%	54.14%
12	3	2	126	0.2046	0.2049	12000	2865.79	0.2388	1.7057	0.3697	15.38%	76.46%
18	3	3	248	0.0755	0.0818	12000	2309.90	0.1925	0.3655	0.1999	81.87%	87.27%

GRU network				GRU Training: Adam BPTT algorithm (GPU)					GRU Validation			
order	layers	units/layer	# param.	RMSE y_1	RMSE y_2	epochs	time	time/epoch	RMSE y_1	RMSE y_2	BFR y_1	BFR y_2
3	1	3	71	0.4960	0.3020	12000	1498.09	0.1248	1.1727	1.3030	41.82%	17.05%
4	1	4	106	0.1376	0.1128	12000	1297.46	0.1081	0.3307	0.2031	83.59%	87.07%
5	1	5	147	0.1617	0.1380	12000	819.22	0.0683	0.1929	0.2127	90.43%	86.46%
7	1	7	247	0.0564	0.0504	12000	810.15	0.0675	0.2219	0.2425	88.99%	84.56%
10	1	10	442	0.0741	0.0853	12000	1460.55	0.1217	0.4643	0.7117	76.96%	54.69%
6	2	3	143	0.2337	0.1584	12000	1578.26	0.1315	0.3226	0.3752	84.00%	76.11%
8	2	4	226	0.1353	0.1265	12000	1581.26	0.1318	0.3751	0.5469	81.39%	65.18%
10	2	5	327	0.0326	0.0309	12000	1591.46	0.1326	0.6165	0.2345	69.41%	85.07%
14	2	7	583	0.0253	0.0325	12000	1571.18	0.1309	0.3244	0.3920	83.91%	75.05%
6	3	2	114	0.1929	0.1647	12000	3638.46	0.3032	0.3943	0.2501	80.44%	84.08%
9	3	3	215	0.0829	0.0858	12000	3741.53	0.3118	0.3664	0.2032	81.83%	87.07%

NNARX network				NNARX Training: Adam BP algorithm (GPU)					NNARX Validation			
order	layers	neuron/layer	# param.	RMSE y_1	RMSE y_2	epochs	time	time/epoch	RMSE y_1	RMSE y_2	BFR y_1	BFR y_2
3	1	5	87	5.0156	4.0211	1000	89.59	0.090	6.3442	3.6032	-214.72%	-129.39%
3	1	8	138	6.8757	6.9953	1000	93.47	0.093	7.2585	6.9879	-260.08%	-344.87%
3	1	10	172	7.8516	7.7647	1000	104.78	0.105	7.7406	9.3001	-284.00%	-492.07%
3	1	15	257	8.0630	9.8919	1000	112.59	0.113	7.4535	10.7121	-269.76%	-581.97%
3	2	3	65	8.2622	9.5509	1000	170.33	0.170	8.1210	9.6828	-302.87%	-516.44%
3	2	5	117	7.7178	9.4936	1000	120.02	0.120	6.6021	9.3484	-227.52%	-495.15%
3	2	7	177	9.9773	8.4243	1000	117.51	0.118	9.8954	8.5393	-390.90%	-443.64%
3	2	10	282	2.5683	5.5859	1000	105.30	0.105	2.0974	5.8676	-4.05%	-273.55%
3	3	3	77	5.4776	3.1718	1000	120.97	0.121	5.5254	2.8112	-174.11%	-78.97%
3	3	5	147	5.3081	5.7561	1000	112.76	0.113	5.2680	6.5923	-161.34%	-319.69%
3	3	7	233	7.6568	9.9372	1000	120.09	0.120	7.5069	11.4208	-272.40%	-627.09%

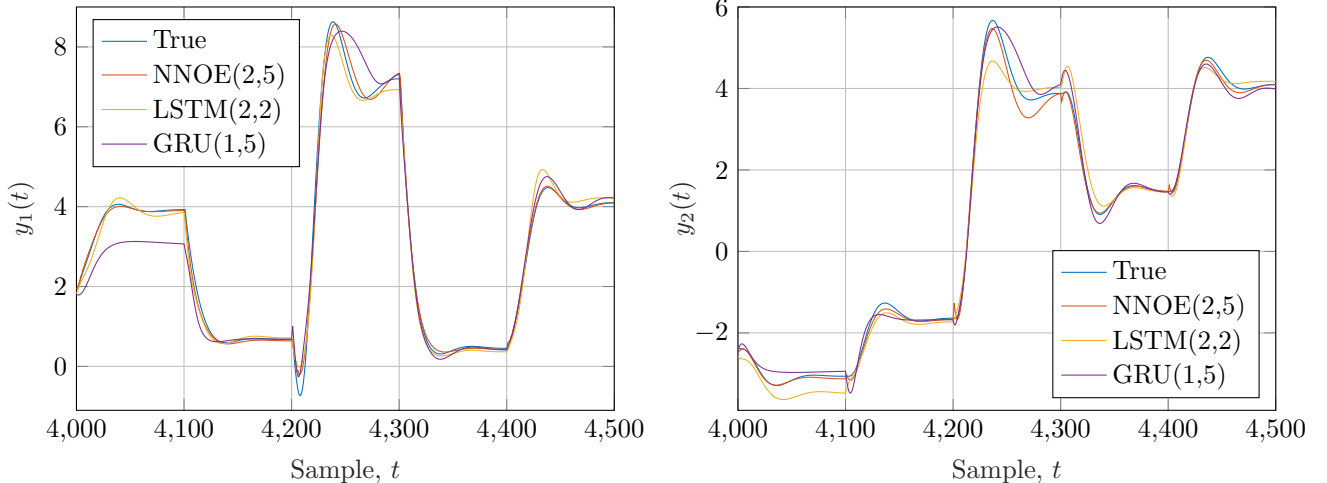


Figure 3: Example 3. Validation output of the top-performing models in each class for output y_1 (left) and y_2 (right).

We apply Algorithm 1 using parameters $K = 2$ and $\tau = 10^{-3}$. For comparison, the system is also identified using the following methods:

1. Least-Squares (LS): The one-step-ahead prediction-error was minimized, resulting in a linear and convex LS problem. The LS approach is widely regarded as the standard method for estimating the physical parameters of dynamical systems, particularly when the system equation depends linearly on the unknown parameters.
2. Adam Backpropagation Through Time (BPTT): The unconstrained SEM optimization problem, as outlined in Equation (6), was formulated and solved using the Adam algorithm. The loss gradient was computed through BPTT, using a learning rate of 10^{-3} , and optimization was conducted over 10^4 epochs.

Table 6: Example 4: Comparison of parameters estimated for the magnetic levitation system using SEM with FL-CMO, SEM with Adam BPTT, and PEM based on LS.

	k_m (H m)	k_0 (N m)
True	2.1039×10^{-4}	0.0
FL-CMO	2.1037×10^{-4}	2.4108×10^{-5}
Adam BPTT	7.46×10^{-4}	-0.143
LS	2.1228×10^{-4}	-3.6130×10^{-4}

We repeat the optimization 10 times for each method, using distinct, zero-mean, normally distributed initializations for the optimization variables. In Table 6, we compare the results of all three methods, selecting the best estimate among all runs for each approach. The results indicate that FL-CMO demonstrates the highest identification accuracy. Although the LS method yields an acceptable estimate, the accuracy of the k_0 parameter is one order of magnitude lower than that of the FL-CMO approach. Conversely, the Adam BPTT method

produces inaccurate estimates for both parameters. We explain these results by observing that, although both FL-CMO and Adam BPTT are based on SEM, Adam BPTT suffers from the vanishing gradient issue.

8 Conclusions

This study investigates system identification for nonlinear input-output models by formulating the simulation-error minimization problem as a constrained optimization task. This formulation avoids vanishing and exploding gradients, which are common issues that hinder convergence in traditional approaches. To solve the constrained problem, we introduce a novel identification algorithm that integrates feedback linearization controlled multipliers optimization with the Euler discretization method, enabling efficient and accurate model estimation.

Our theoretical analysis provides guarantees of local convergence and establishes connections between the proposed approach and the conventional unconstrained formulation. By leveraging the problem structure and employing sparse Q-less QR factorization, we reduce the computational complexity of the iterative process compared to standard unconstrained optimization techniques.

Extensive numerical experiments on black-box and gray-box problems reveal that the proposed approach outperforms conventional methods. Additionally, we find that adequately trained neural input-output models can exhibit superior performance compared to state-space neural ones, such as LSTM and GRU. These findings offer an efficient alternative to gradient-based identification methods for nonlinear systems. Future research will focus on developing solutions to further enhance efficiency in large-scale problems.

References

- [Adeoye and Bemporad, 2024] Adeoye, A. D. and Bemporad, A. (2024). An inexact sequential quadratic programming method for learning and control of recurrent neural networks. IEEE Trans. Neural Netw. Learn. Syst., pages 1–15.
- [Bas et al., 2022] Bas, E., Egrioglu, E., and Kolemen, E. (2022). Training simple recurrent deep artificial neural network for forecasting using particle swarm optimization. Granul. Comput., 7(2):411–420.
- [Baydin et al., 2018] Baydin, A. G., Pearlmutter, B. A., Radul, A. A., and Siskind, J. M. (2018). Automatic differentiation in machine learning: a survey. J. Mach. Learn. Res., 18:1–43.
- [Belz et al., 2017] Belz, J., Münker, T., Heinz, T. O., Kampmann, G., and Nelles, O. (2017). Automatic modeling with local model networks for benchmark processes. In IFAC World Congress, volume 50, pages 470–475.
- [Bemporad, 2022] Bemporad, A. (2022). Recurrent neural network training with convex loss and regularization functions by extended kalman filtering. IEEE Trans. Autom. Control, 68(9):5661–5668.
- [Bemporad, 2025] Bemporad, A. (2025). An L-BFGS-B approach for linear and nonlinear system identification under ℓ_1 and group-lasso regularization. IEEE Trans. Autom. Control, 70(7):4857–4864.
- [Bengio et al., 1994] Bengio, Y., Simard, P., and Frasconi, P. (1994). Learning long-term dependencies with gradient descent is difficult. IEEE Trans. Neural Netw., 5(2):157–166.
- [Blanco et al., 2001] Blanco, A., Delgado, M., and Pegalajar, M. C. (2001). A real-coded genetic algorithm for training recurrent neural networks. Neural Netw., 14(1):93–105.
- [Bohlin, 2006] Bohlin, T. P. (2006). Practical grey-box process identification: theory and applications. Springer Science & Business Media.
- [Centorrino et al., 2025] Centorrino, V., Rossi, F., Bullo, F., and Russo, G. (2025). Proximal gradient dynamics and feedback control for equality-constrained composite optimization.
- [Cerone et al., 2023] Cerone, V., Fosson, S. M., Pirrera, S., and Regruto, D. (2023). Alternating direction method of multipliers for polynomial optimization. In Eur. Control Conf. (ECC), pages 1–6.
- [Cerone et al., 2024] Cerone, V., Fosson, S. M., Pirrera, S., and Regruto, D. (2024). A feedback control approach to convex optimization with inequality constraints. In IEEE Conf. Decis. Control (CDC), pages 2538–2543.
- [Cerone et al., 2025] Cerone, V., Fosson, S. M., Pirrera, S., and Regruto, D. (2025). A new framework for constrained optimization via feedback control of lagrange multipliers. IEEE Trans. Autom. Control, 70(11):7141–7156.
- [Cerone et al., 2014] Cerone, V., Lasserre, J.-B., Piga, D., and Regruto, D. (2014). A unified framework for solving a general class of conditional and robust set-membership estimation problems. IEEE Trans. Autom. Control, 59(11):2897–2909.
- [Cerone et al., 2012] Cerone, V., Piga, D., and Regruto, D. (2012). Set-membership error-in-variables identification through convex relaxation techniques. IEEE Trans. Autom. Control, 57(2):517–522.
- [Chollet et al., 2015] Chollet, F. et al. (2015). Keras. <https://github.com/keras-team/keras>.
- [Conte et al., 1999] Conte, G., Moog, C. H., and Perdon, A. M. (1999). Nonlinear control systems: An algebraic setting, volume 242. Springer.
- [Davis, 2011] Davis, T. A. (2011). Algorithm 915, suitesparseqr: Multifrontal multithreaded rank-revealing sparse QR factorization. ACM Trans. Math. Softw., 38(1):1–22.
- [Esfahani et al., 2017] Esfahani, A. F., Dreesen, P., Tiels, K., Noël, J.-P., and Schoukens, J. (2017). Polynomial state-space model decoupling for the identification of hysteretic systems. In IFAC World Congr., pages 458–463.
- [Farina and Piroddi, 2010] Farina, M. and Piroddi, L. (2010). Convergence properties of an iterative prediction approach to nonlinear sem parameter estimation. In IEEE Conf. Decis. Control (CDC), pages 7226–7231. IEEE.
- [Farina and Piroddi, 2011] Farina, M. and Piroddi, L. (2011). Simulation error minimization identification based on multi-stage prediction. Int. J. Adapt. Control Signal Process., 25(5):389–406.
- [Forgione and Piga, 2021] Forgione, M. and Piga, D. (2021). dynoNet: A neural network architecture for learning dynamical systems. Int. J. Adapt. Control Signal Process., 35(4):612–626.
- [Isidori, 1995] Isidori, A. (1995). Nonlinear Control Systems. Springer London.
- [Khalil, 2002] Khalil, H. K. (2002). Nonlinear Systems. Pearson Education. Prentice Hall, 3rd edition.
- [Laue et al., 2018] Laue, S., Mitterreiter, M., and Giesen, J. (2018). Computing higher order derivatives of matrix and tensor expressions. In Adv. Neural Inf. Process. Syst. (NIPS), volume 31.
- [Liu et al., 2018] Liu, X., Liu, S., Sha, J., Yu, J., Xu, Z., Chen, X., and Meng, H. (2018). Limited-memory BFGS optimization of recurrent neural network language models for speech recognition. In Int. Conf. Acoust. Speech Signal Process. (ICASSP), pages 6114–6118. IEEE.

- [Ljung, 1999] Ljung, L. (1999). System Identification: Theory for the User. Prentice Hall PTR.
- [Medsker and Jain, 1999] Medsker, L. and Jain, L. C. (1999). Recurrent neural networks: design and applications. CRC press.
- [Milanese et al., 1996] Milanese, M., Norton, J., Piet-Lahanier, H., and Walter, É. (1996). Bounding Approaches to System Identification. Springer US.
- [Milanese and Novara, 2004] Milanese, M. and Novara, C. (2004). Set membership identification of nonlinear systems. Automatica, 40(6):957–975.
- [Mirikitani and Nikolaev, 2009] Mirikitani, D. T. and Nikolaev, N. (2009). Recursive Bayesian recurrent neural networks for time-series modeling. IEEE Trans. Neural Netw., 21(2):262–274.
- [Narendra and Parthasarathy, 1991] Narendra, K. and Parthasarathy, K. (1991). Gradient methods for the optimization of dynamical systems containing neural networks. IEEE Trans. Neural Netw., 2(2):252–262.
- [Noel and Schoukens, 2016] Noel, J.-P. and Schoukens, M. (2016). Hysteretic benchmark with a dynamic nonlinearity. In Workshop on nonlinear system identification benchmarks, pages 7–14.
- [Nørgård et al., 1996] Nørgård, P. M., Ravn, O., Hansen, L. K., and Poulsen, N. K. (1996). The nnsysid toolbox - a matlab toolbox for system identification with neural networks. In IEEE Symp. Comput.-Aided Control Syst. Des., pages 374–379. IEEE.
- [Parrilo and Ljung, 2003] Parrilo, P. A. and Ljung, L. (2003). Initialization of physical parameter estimates. In IFAC Symp. Syst. Identif. (SYSID), pages 1483–1488.
- [Pascanu et al., 2013] Pascanu, R., Mikolov, T., and Bengio, Y. (2013). On the difficulty of training recurrent neural networks. In Int. Conf. Mach. Learn. (ICLM), pages 1310–1318.
- [Peng and Magoulas, 2011] Peng, C.-C. and Magoulas, G. (2011). Nonmonotone BFGS-trained recurrent neural networks for temporal sequence processing. Appl. Math. Comput., 217(12):5421–5441.
- [Piroddi, 2008] Piroddi, L. (2008). Simulation error minimisation methods for narx model identification. Int. J. Model. Identif. Control, 3(4):392–403.
- [Piroddi and Spinelli, 2003] Piroddi, L. and Spinelli, W. (2003). An identification algorithm for polynomial narx models based on simulation error minimization. Int. J. Control, 76(17):1767–1781.
- [Prot and Mercère, 2020] Prot, O. and Mercère, G. (2020). Combining linear algebra and numerical optimization for gray-box affine state-space model identification. IEEE Trans. Autom. Control, 65(8):3272–3285.
- [Ramaswamy, 2023] Ramaswamy, A. (2023). Gradient clipping in deep learning: A dynamical systems perspective. In Int. Conf. Pattern Recognit. Appl. Methods (ICPRAM), volume 1, pages 107–114.
- [Ruder, 2016] Ruder, S. (2016). An overview of gradient descent optimization algorithms. arXiv preprint arXiv:1609.04747.
- [Salem, 2022] Salem, F. M. (2022). Recurrent Neural Networks. Springer.
- [Sjöberg et al., 1994] Sjöberg, J., Hjalmarsson, H., and Ljung, L. (1994). Neural networks in system identification. In IFAC Symp. Syst. Identif. (SYSID), pages 359–382.
- [Söderström and Stoica, 1982] Söderström, T. and Stoica, P. (1982). Some properties of the output error method. Automatica, 18(1):93–99.
- [Stewart, 1998] Stewart, G. W. (1998). Matrix algorithms: volume 1: basic decompositions. SIAM.
- [Sundnes, 2024] Sundnes, J. (2024). Solving Ordinary Differential Equations in Python. Springer Nature Switzerland.
- [Wang et al., 2009] Wang, J., Sano, A., Chen, T., and Huang, B. (2009). Identification of hammerstein systems without explicit parameterisation of nonlinearity. Int. J. Control, 82(5):937–952.
- [Wanner and Hairer, 1996] Wanner, G. and Hairer, E. (1996). Solving ordinary differential equations II, volume 375. Springer Berlin Heidelberg New York.
- [Williams and Zipser, 1990] Williams, R. J. and Zipser, D. (1990). Gradient-based learning algorithms for recurrent connectionist networks. Citeseer.
- [Zhang, 2004] Zhang, Q. (2004). Nonlinear system identification with output error model through stabilized simulation. In IFAC Symp. Nonlinear Control Syst. (NOLCOS), pages 501–506.